DOI 10.24425/aee.2024.148867

Effect of surface energy on the contamination characteristics of porcelain double umbrella insulators

YUKUN LV, QIAN WANG✉, ZEZE CHEN, JIAWEN WANG

Department of Power Engineering, North China Electric Power University
China
e-mail: twfx15049293556@163.com

(Received: 17.09.2023, revised: 01.03.2024)

Abstract: To explore the influence of surface energy on the contamination characteristics of insulators, COMSOL Multiphysics software was used to simulate the contamination characteristics of XWP_2-160 insulators under wind tunnel conditions, and the rationality of the modified expression of the dynamic deposition model of the contaminated particles was verified. The change of contamination characteristics before and after changing the surface energy of insulators under natural conditions was simulated and analyzed. The results show that under the original surface energy (72 mJ/m^2) and low surface energy (6.7 mJ/m^2) with the increase in particle size, the contamination amount of an insulator surface area decreases first and then increases. When the wind speed is 2 m/s, the change in the particle size has the most pronounced effect on the amount of contamination. The amounts of contamination for the low surface energy are 64–75%, 60–95%, 55–91% and 54–78% lower than those for the original surface energy for particle sizes of 10, 15, 20 and 25 μm, respectively. For the same wind speed, when the size of contamination particles increases, the difference between the ratio of DC and AC contamination accumulation is gradually increasing because of the influence of the electric field force. From the perspective of the insulator preparation process, the development of low surface energy insulators can improve their anti-fouling performance.

Key words: contamination characteristics, numerical simulation, surface energy, XWP_2-160 insulator

1. Introduction

Insulators are extensively used in transmission lines due to their good insulation performance [1–3]. Differences between insulator materials lead to differences in contamination particle aggregation [4] and the surface energy of the insulator, which describes the energy state of the

© 2024. The Author(s). This is an open-access article distributed under the terms of the Creative Commons Attribution-NonCommercial-NoDerivatives License (CC BY-NC-ND 4.0, https://creativecommons.org/licenses/by-nc-nd/4.0/), which permits use, distribution, and reproduction in any medium, provided that the Article is properly cited, the use is non-commercial, and no modifications or adaptations are made.

surface as well as directly affects its contamination accumulation characteristics [5]. Therefore, understanding the influence of insulator surface energy on contamination characteristics under natural conditions can provide guidance for the study of insulator shed surface materials and the effective reduction of the degree of insulator contamination.

Li [5] explored the influence of the material composition of the ceramic sample on the surface energy, and concluded that the silicon-aluminum ratio has a strong influence on the surface energy of the ceramic. A higher surface energy of the ceramic corresponds to a greater contact angle between the oil droplet and its surface and to a smaller work of adhesion. Hu [6] used the contact angle method to study the ease of cleaning ceramic glazes. The measurement results showed that the surface energy increases with a higher proportion of polar components, which also corresponds to a greater cleanliness of ceramic products. Wang [7] used atomic force microscopy to study the adhesion force of different materials from a microscopic point of view. The results showed that the adhesion force is related to material properties, surface roughness and surface charge. Xu [8] fabricated a composite ceramic film layer, observed and analyzed the micro morphology, elemental composition, roughness, and phase composition of the composite ceramic film layer, and pointed out that due to the formation of a large number of grains on the material surface, the specific surface area crystal defects increased, leading to an increase in roughness and ultimately improving the surface energy of the film layer. Jiang [9] explored the particle size distribution characteristics of contamination particles through natural contamination accumulation experiments and transmission line experiments. The results showed that the relative humidity and wind speed on the surface of porcelain insulators have a significant impact on the particle size distribution, and the particles with sizes in the 20–80 μm range are most affected by the correlation parameters. Zhang [10] used an artificial aerosol chamber to carry out contamination tests and verified that the material type and other factors had an important influence on the distribution of contamination morphology on the insulator surface. He [11] collected pollutants and measured their chemical composition through a natural pollution monitoring platform. The results showed that both the equivalent salt deposit density (ESDD) and non-soluble deposit density (NSDD) of the de-energized insulator on the tower decrease with the increase in height, but then decrease slowly. Gao [12] cleaned different types of contaminated insulators in natural rainfall. The results showed that the washing effect of natural rainfall on the surface contamination of different umbrella skirts is not consistent, and contamination with particle sizes less than 25 μm and greater than 300 μm is more likely to be washed by natural rainfall. Zhang [13] established a hydrodynamic model of a typical shed insulator and compared it with the natural pollution tests. The study found that the particle collision coefficient was affected by the particle size and wind speed, and there was a maximum value. After considering the effect of rainfall, the pollution effects on different umbrella insulators were summarized. Tu [14] tested four types of insulators under three different voltages and counted the particle size of the contaminated particles in the haze environment. Natural contamination tests were conducted on four types of insulators under three voltages in a haze environment, and the size distribution of the contamination particles was determined. The results showed that the particle size of the contamination particles deposited on the surface of the insulator under the haze environment has a lognormal distribution, and the particle size distributions of the contamination particles under the three voltage conditions are quite different.

The above studies have performed a lot of much work in the study of insulator contamination characteristics and analyzed the influence of different environmental factors on the contamination

amount and contamination state of the skirt surfaces in detail. Nevertheless, there are few studies on the influence of the energy state of insulator shed material on the contamination characteristics of insulators. Therefore, this article takes the XWP_2-160 porcelain double umbrella insulator as a research object to explore the influence of surface energy change on insulator contamination characteristics in natural environments.

2. Physical field control equation and deposition model correction

2.1. Flow field control equation

When fluid flows through the insulator wall, the streamline changes due to its shape. Due to the low flow rate, the pressure changes little. According to the principles of viscous fluid mechanics, the air is regarded as an incompressible viscous fluid in the flow field simulation, and the Lagrange model is used to simulate the gas-solid two-phase flow. Taking into account the fact that the streamline is prone to bending when the airflow flows through the insulator, the RNG k–ε model is used to improve the calculation accuracy of the flow field [15]. The governing equations are as follows:

$$\begin{cases} \rho(\boldsymbol{U}\cdot\nabla)\boldsymbol{U} = \nabla\cdot\left[-\rho\boldsymbol{I} + (\mu+\mu_{\mathrm{T}})\left(\nabla\boldsymbol{U} + (\nabla\boldsymbol{U})^{\mathrm{T}}\right) - \dfrac{2}{3}\rho k\boldsymbol{I}\right] + \boldsymbol{F} \\ \nabla\cdot\boldsymbol{U} = 0 \\ \rho(\boldsymbol{U}\cdot\nabla)k = \nabla\cdot\left[\left(\mu + \dfrac{\mu_{\mathrm{T}}}{\sigma_{\mathrm{k}}}\right)\nabla k\right] + P_{\mathrm{k}} - \rho\varepsilon \\ \rho(\boldsymbol{U}\cdot\nabla)\varepsilon = \nabla\cdot\left[\left(\mu + \dfrac{\mu_{\mathrm{T}}}{\sigma_{\varepsilon}}\right)\nabla\varepsilon\right] + C_{\varepsilon 1}\dfrac{\varepsilon}{k}P_{\mathrm{k}} - C_{\varepsilon 2}\rho\dfrac{\varepsilon^2}{k} \\ \mu_{\mathrm{T}} = \rho C_{\mu}\dfrac{k^2}{\varepsilon} \\ P_{\mathrm{k}} = \mu_{\mathrm{T}}\left[\nabla\boldsymbol{U} : \left(\nabla\boldsymbol{U} + (\nabla\mathbf{U})^{\mathrm{T}}\right)\right] \end{cases}, \tag{1}$$

where: $\boldsymbol{U}$ is the velocity of the flow field; $\boldsymbol{I}$ is the main stress tensor; μ is the aerodynamic viscosity; μ_{T} is the turbulent dynamic viscosity; ρ is the air density; $\boldsymbol{F}$ is the volume force; k is the turbulent kinetic energy; ε is the turbulent dissipation rate; C_{μ} is the viscosity coefficient, σ_{k}, σ_{ε}, $C_{\varepsilon 1}$, and $C_{\varepsilon 2}$ are turbulence parameters, and P_{k} is the turbulent energy term.

2.2. Electric field control equation

In the numerical simulation, the steady-state analysis method is adopted for the DC electric field, and its control equation is:

$$\begin{cases} \nabla\cdot\boldsymbol{D} = \rho_{\mathrm{v}} \\ \boldsymbol{E} = -\nabla V \\ \boldsymbol{D} = \varepsilon_0\varepsilon_0'\boldsymbol{E} \end{cases}, \tag{2}$$

where: $\boldsymbol{E}$ is the electric field strength; $\boldsymbol{D}$ is the electric displacement; V is the electric potential; ε_0 is the vacuum permittivity; ε_0' is the relative permittivity of the material, and ρ_{v} is the bulk charge density.

2.3. Particle field control equation

The size of the contamination particles studied in this paper is on the order of microns, forming a dilute phase with air; the influence of the particles on the flow field is ignored. Therefore, the following settings are used:

1. the contamination particles are spherical;
2. the particle blowing velocity is the same as the flow velocity; and
3. the secondary forces (e.g. dielectrophoretic force and interparticle interaction force [16]) on the particles are ignored.

In the particle field (particle tracking) module, the force of the contaminated particles can be described as:

$$\frac{m_{\mathrm{p}}\mathrm{d}\boldsymbol{v}}{\mathrm{d}t} = \boldsymbol{F}_{\mathrm{e}} + \boldsymbol{F}_{\mathrm{g}} + \boldsymbol{F}_{\mathrm{d}}, \tag{3}$$

where: m_{p} is the quality of the contaminated particles; $\boldsymbol{v}$ is the velocity of the contamination particles; t is the movement time of the contamination particles, and $\boldsymbol{F}_{\mathrm{e}}$, $\boldsymbol{F}_{\mathrm{g}}$, $\boldsymbol{F}_{\mathrm{d}}$ are the electric field force, gravity and fluid drag force on the contamination particles, respectively.

2.4. Modification of the dynamic deposition model of contaminated particles

Due to the effect of unbalanced force, solid surface molecules are prone to produce inwards contraction force or potential energy, that is, there exists a surface energy (for solids) or surface tension (for liquids). Considering that the surface energy is the macroscopic characteristic of the material, it has a direct impact on the collision and adhesion process between the particles and the insulator surface, which cannot be ignored. The adsorption effect of the surface energy of the insulator shed on the contaminated particles is similar to the adhesion force, so it is considered to set the direction of action as the normal direction. Specifically, the surface energy R is added to supplement the normal discriminant of the original deposition model [17]. The modified deposition model is as follows:

$$\left.\begin{array}{l} \boldsymbol{n}: R + \boldsymbol{F}_{\mathrm{a}} l_{\mathrm{a}} + E_{\mathrm{p}} \cos^2\theta + \boldsymbol{F}_{\mathrm{g}} l_{\mathrm{g}} \cos\theta - (\boldsymbol{F}_{\mathrm{p}} l_{\mathrm{p}} + E_{\mathrm{s}} E_{\theta} q l_{\mathrm{e}}) \geq 0 \\ \boldsymbol{t}: \left\{ \begin{array}{l} qE_{\mathrm{s}} E_{tx} l_{\mathrm{f}} + E_{\mathrm{p}} \sin^2\theta \cos^2\phi \leq \boldsymbol{F}_{\mathrm{f}} l_{\mathrm{f}} \\ qE_{\mathrm{s}} E_{ty} l_{\mathrm{f}} + E_{\mathrm{p}} \sin^2\theta \sin^2\phi \leq \boldsymbol{F}_{\mathrm{f}} l_{\mathrm{f}} \end{array} \right. \end{array}\right\}, \tag{4}$$

$$R = A\sqrt{r_1 r_2}, \tag{5}$$

where: l_{a}, l_{p}, l_{f}, l_{g} and l_{e} are the corresponding distances for each force (the forces are the adhesion force, the collision force, the friction force, gravity and the electric field force); E_{s} is the magnitude of the field strength vector of the collision point; E_{p} is the kinetic energy before particle collision; in the spherical coordinate system (r, θ, ϕ) with the particle collision point as the origin, θ and ϕ are the direction angle coordinates; r_1 is the surface energy of the contaminated particles; r_2 is the surface energy of the insulator shed surface, and A is the area of the contact surface.

3. Rationality verification of the numerical simulation method

3.1. Introduction of wind tunnel contamination test

To verify the validity of the model, the contamination tests were carried out in the wind tunnel laboratory of North China Electric Power University (NCEPU) [18]. Figure 1 shows a structural diagram of the wind tunnel test system. The wind tunnel test is conducted for the

breeze environment in the atmosphere (the wind speed is close to 4 m/s). Because the influence of rainwater erosion is not considered, the low-speed section of the test system is selected (length, width and height of 10.5, 1.1 and 0.8 m).

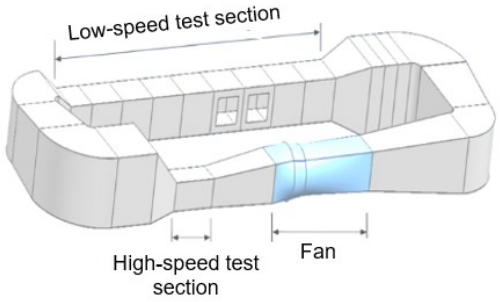

Fig. 1. Schematic diagram of wind tunnel test structure

The XWP_2-160 porcelain double umbrella insulators were selected for the wind tunnel test. Figure 2 shows a schematic diagram of the structural parameters of the insulator, and the measured creepage distance is 450 mm. Due to the limitation of the height of the low-speed experimental section, according to the structural parameters of the insulator single shed, four porcelain double umbrella insulators were selected as the research object.

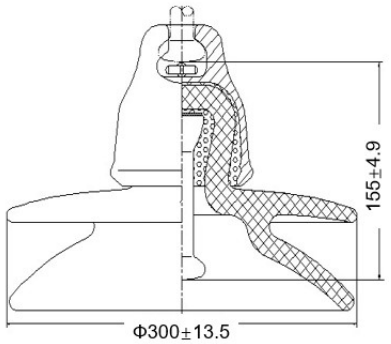

Fig. 2. Structure parameter diagram of XWP_2-160 porcelain double umbrella insulator

The DC voltage level is set to 0, ±12, ±18, ±24, ±30, ±36 kV. The contamination state of insulators under different voltage levels was investigated by testing. The sample consists of sand, diatomite, and NaCl particles mixed at a ratio of 6:6:1 [19]. The sizes of the sand, diatomite, and NaCl particles were approximately 100, 50, and 100 μm, and their densities were 2.32, 0.47 and 2.165 g/cm^3. Because the value of the salt density of the insulator surface in the wind tunnel test has been maintained at approximately 287 μg/cm^2, there is no evident change; therefore, the NSDD (non-soluble deposit density) value is selected as the evaluation index of the insulator contamination characteristics.

3.2. Numerical simulation of the wind tunnel test

According to the dimensions of the equipment in the low-speed section of the test, COMSOL Multiphysics software is used to construct the calculation model, as shown in Fig. 3. For a more accurate simulation of the electric field distribution around the insulator, an "infinite element field" is constructed outside the rectangular computational region for the absorption of reflected electromagnetic waves. The flow field region includes the velocity inlet on the front side, the pressure outlet on the back side, four adjacent surfaces (all set as turbulent steady state walls) and the insulator. In the computational domain of the flow field, the velocity inlet, outlet and walls are the outer boundary conditions and the inner boundary of the "infinite element field". The fluid velocity and pressure distribution near the insulator surface are calculated by the wall function in the software. The fluid in the flow field is set to be incompressible, and the density and kinetic viscosity are derived from the material. The particle field is the same as the flow field region, and the particle deposition on the insulator surfaces is modelled according to Eqs. (4–5). Based on the wind tunnel test data, the particle blowing speed of the front side inlet is set to be 4 m/s.

The shed material of the porcelain double umbrella insulator is porcelain clay, feldspar and quartz, and its main chemical composition is 70% SiO_2 and 20% Al_2O_3, with a silica-aluminum ratio of approximately 3.5 [20]. The surface energy values are different for different silica-aluminum ratios in porcelain parts [5]. According to reference [21], the surface energy of the shed of the porcelain double umbrella insulators is 72 mJ/m^2.

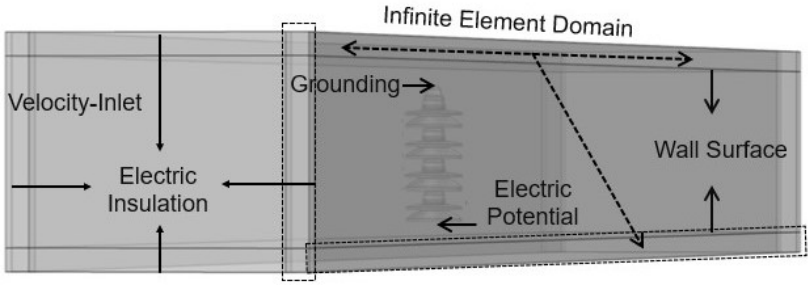

Fig. 3. Geometric physical model and boundary conditions of low-speed section in wind tunnel test

3.3. Comparative analysis of simulation and test results

Figure 4 compares the wind tunnel test results and simulation results for porcelain double umbrella insulators. After correcting the original deposition model using the surface energy, the comparison between the simulation and the wind tunnel test results shows that the both results have the same magnitudes and exhibit similar variation trend of the fouling curve, validating the method used for the simulation of insulator contamination characteristics. Under a positive polarity voltage, the average relative error between the modified deposition model and the test is 11%, which is clearly smaller than the deviation of the original deposition model from the test results. However, under the action of negative polarity voltage, a larger error occurs, which may be attributed to the following: numerical simulation uses a somewhat simplified insulator model, and there are

differences in the spatial flow field compared with the wind tunnel test; only diatomaceous earth is selected in the simulation, and the particle model is simplified compared with the proportionally mixed contamination samples used in the test; the effect of the negative polarity voltage on the contamination is relatively weak, while the surface energy term in the modified model directly amplifies its effect on the contamination. The surface energy term in the modified model directly amplifies its effect on contamination. Comparing the simulation and test results, the error is within a reasonable range. Therefore, it is concluded that the numerical simulation method using the modified model can accurately simulate the contamination characteristics of porcelain double umbrella insulators.

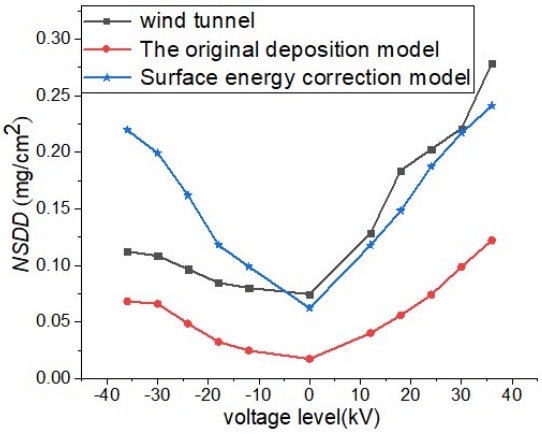

Fig. 4. Comparison of wind tunnel test and simulation results of porcelain double umbrella insulators

4. Numerical simulation of the influence of surface energy on the insulator contamination characteristics

For a more intuitive analysis of the influence of different surface energy on insulator contamination, two surface energy conditions are defined as follows:

1. The surface energy of the porcelain double umbrella insulators is calculated as described in 2.2 (original surface energy);
2. When the contact angle is greater than 120°, the porcelain has low surface energy and exhibits superhydrophobicity [22, 23], that is, good stain resistance.

The minimum surface energy of the porcelain double umbrella insulator shed surfaces may be 6.7 mJ/m^2 (low surface energy).

On the basis of the modified model, considering the conditions of the original surface energy and low surface energy (expressed by r_O and r_L, respectively) of the insulator shed calculated above, the natural contamination characteristics of the XWP$_2$-160 porcelain double umbrella insulators under 110 kV DC voltage are numerically simulated.

4.1. Wind speed and particle size analysis

The composition of the pollution particles in the environment is more complex. To determine the size of the contamination particles used in the simulation study, the particle size of the air contamination particles in the Hebei province was measured using a Mastersizer 3 000 laser particle size analyzer. The results are shown in Fig. 5. According to the measurement results, the size of the air contamination particles is mostly concentrated in the 5–40 μm range.

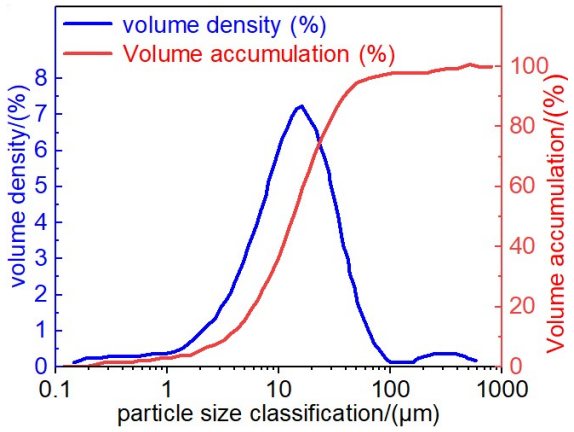

Fig. 5. Particle size distribution

An AS8336 split digital anemometer was used to measure the wind speed at an approximate height of the high-voltage transmission tower. The results of multiple measurements showed that the wind speed range is 0–5 m/s. The wind speed will be reasonably selected according to the measurement results of the breeze environment in the follow-up study.

4.2. Setting of monodromic conditions

According to the arrangement rule of the transmission line insulator under different voltage levels, seven pieces of XWP_2-160 porcelain double umbrella insulators were selected for the study, corresponding to the voltage level of the actual 110 kV transmission line. The insulator model setup is similar to the physical model of the wind tunnel test, but to better represent more in line with the actual part of the setup, the following adjustments were made: the four walls of the fluid domain were set to 'symmetrical' in the numerical simulation of natural pollution. The proportions of positive and negative charges carried by dirty particles were set to approximately 31% and 26%, with an average charge corresponding to 6.3×10^{-6} C/g and -7×10^{-6} C/g [24]. To investigate the variation in the insulator contamination with particle size, wind speed and contamination concentration under two surface energy values, the sizes of the contamination particles were set to 10, 15, 20 and 25 μm, and the wind speeds were set to 1, 2, 3 and 4 m/s. The contamination concentrations were 0.15, 0.30 and 0.45 mg/m^3.

4.3. Analysis of flow field simulation results

Taking natural pollution (wind speed is 2 m/s) as an example, the simulation results of the flow field were analyzed, as shown in Fig. 6.

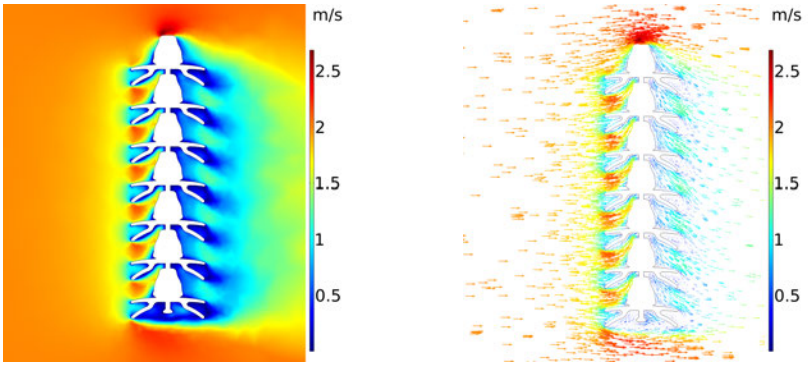

(a) (b)

Fig. 6. Flow field simulation results diagram: velocity contour (a); vector diagram of flow field velocity (b)

As shown in Fig. 6(a), the separation of the boundary layer occurs on the leeward side of the insulator. Figure 6(a) shows that the airflow velocity on the upper surface of the shed on the windward side of the insulator is higher, whereas the velocity on the lower surface of the shed is lower than the mainstream velocity in the space. From Fig. 6(b), the space between the two sheds of the insulator forms a large counterclockwise vortex and a negative pressure core, which more easily entangles the contamination particles. The flow field simulation results are consistent with the viscous hydrodynamic theory, indicating that the insulator natural contamination simulation results are consistent with the actual situation.

4.4. Analysis of the influence of the surface energy on the contamination characteristics of porcelain double umbrella insulators

4.4.1. The change in the contamination amount with particle size for two kinds of surface energy

The gravity, electric field force and fluid drag force of the contamination particles are closely related to their particle size. Figure 7 shows the change in the contamination amount with particle size for two kinds of surface energy.

As shown in Fig. 7, the amount of contamination on the insulator surface first decreases and then increases with increasing particle size for two kinds of surface energy. The comparison of the subfigures in Fig. 7 shows that when the wind speed is 2 m/s, the change in particle size has the most pronounced effect on the amount of contamination, which is shown as follows: compared with the 10 μm particle size, the amounts of contamination for the original surface energy and the low surface energy of the 15 μm particle size decreases by approximately 60–81% and 80–93%, respectively, and the reduction rate of the low surface energy shed contamination is larger than that for the original surface energy under the same contamination concentration. The reduction in the amount of the contamination in the low surface energy shed was larger than that for the original

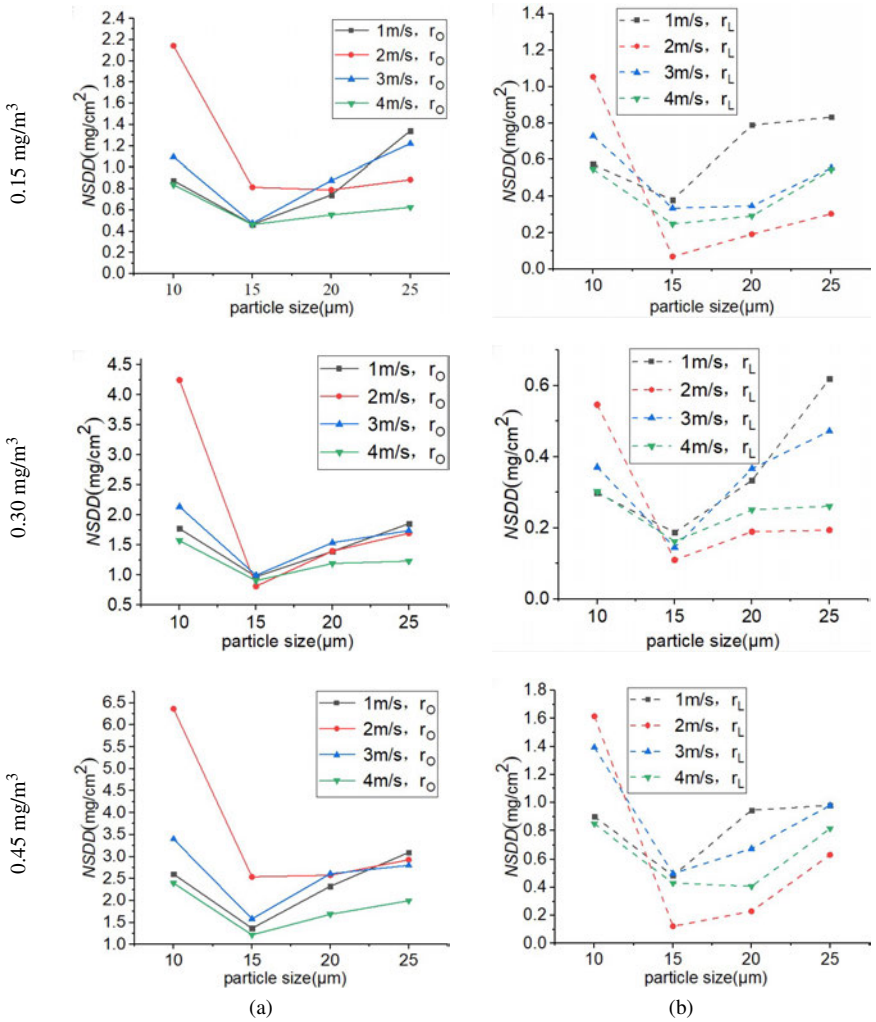

Fig. 7. The change in the contamination amount with particle size for two kinds of surface energy: original surface energy (a); low surface energy (b)

surface energy. Under the same wind speed, the settling forces of the particles of different sizes are different, and when the contamination particles collide with the shed, due to the low surface energy, the attraction to the particles in the normal direction is relatively weak [25], leading to the above-described behavior. The amounts of contamination for the low surface energy are 64–75%, 60–95%, 55–91% and 54–78% lower than those for the original surface energy for particle sizes of 10, 15, 20 and 25 μm. For the low surface energy, the amounts of shed contamination were greatly reduced, and this effect was more pronounced for the larger size of the contamination particles (>10 μm). Therefore, the method of reducing the surface energy of the shed can effectively address the problem of insulator contamination.

4.4.2. The change in the contamination amount with wind speed for two kinds of surface energy

The voltage type directly affects the size and direction of the electric field force in the particle movement, resulting in a change in the trajectory of the particle, and a large difference in contamination under different voltage types. Figure 8 shows the variation of contamination amount with wind speed under two kinds of surface energy.

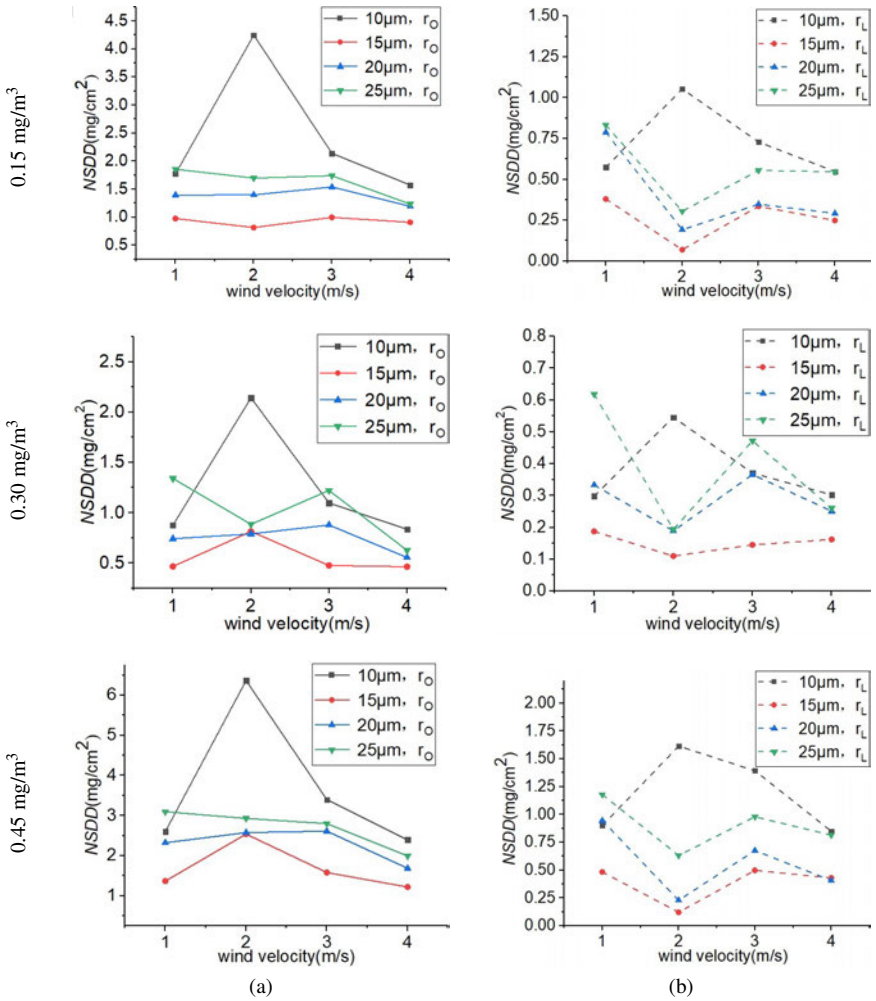

Fig. 8. The variation of contamination amount with wind speed under two kinds of surface energy: original surface energy (a); low surface energy (b)

As seen from Fig. 8, for small particle sizes (10 μm), the trends for both the original surface energy and the low surface energy contamination with wind speed are basically the same. For larger particle sizes (>10 μm), there is no uniform law in the variation of the amount of contamination for the two kinds of surface energy with wind speed because the increase in particle size makes

the inertia and randomness of particles increase. With the increase in wind speed, the carrying capacity of the fluid is also enhanced. The likelihood of some particles bouncing off the metal fixture and depositing on the surface of the shed is uncertain because of the influence of these two conditions, resulting in inconsistent patterns. For two kinds of surface energy, the contamination of 10 μm particles is most evidently affected by the wind speed. The contamination curve exhibits a pronounced transition when the wind speed is 2 m/s. At this wind speed, the fouling curve reaches the maximum value for the original surface energy and the minimum value for the low surface energy, indicating that the surface energy exerts a strong effect on this condition.

The comparison of subfigures in Fig. 8 shows that the amount of contamination increases with increasing contamination concentration for both surface energy; however, a difference in the magnitude of the growth rate is observed. When the surface energy is reduced, the amount of contamination decreases by approximately 59–95% at larger particle sizes and higher contamination concentrations (> 0.30 mg/m^3) for the low surface energy compared to the original surface energy.

4.4.3. The change in the contamination amount with voltage type for two kinds of surface energy

The type of voltage affects the distribution of the electric field near the insulator and the size and direction of the electric field force on the particles, leading to changes in the trajectory of the particles, and a large difference in the contamination under different voltage types. Table 1 shows the comparison of contamination amount for different surface energy and voltage types when the contamination concentration is 0.15 mg/m^3.

Table 1. Comparison of contamination amount for different surface energy and voltage types

Particle Size (μm)	**1m/s**		**2m/s**		**3m/s**		**4m/s**	
	NSDD$_{DC}$	**NSDD$_{AC}$**	**NSDD$_{DC}$**	**NSDD$_{AC}$**	**NSDD$_{DC}$**	**NSDD$_{AC}$**	**NSDD$_{DC}$**	**NSDD$_{AC}$**
10(r_O)	0.8765	0.2273	2.1426	0.5808	1.0970	0.8755	0.8364	0.7198
10(r_L)	0.2983	0.1039	0.5460	0.2891	0.3706	0.3209	0.3024	0.2706
15(r_O)	0.4667	0.1203	0.8148	0.4287	0.4756	0.1859	0.4635	0.3105
15(r_L)	0.1875	0.0045	0.1099	0.0616	0.1454	0.0766	0.1623	0.1006
20(r_O)	0.7421	0.1114	0.7901	0.2103	0.8790	0.4454	0.5555	0.3325
20(r_L)	0.3333	0.0808	0.1893	0.0721	0.3663	0.2057	0.2510	0.1439
25(r_O)	1.3409	0.1867	0.8856	0.2542	1.2219	0.3728	0.6262	0.2132
25(r_L)	0.6183	0.1350	0.1938	0.0551	0.4719	0.1393	0.2606	0.0978

As shown in Table 1, compared to the amount of contamination of insulators under the action of AC voltage, the amount of contamination under the action of DC voltage is significantly higher. With increasing wind speed, the difference between the amount of contamination under DC and AC voltages gradually decreases, and the minimum difference in the amount of contamination is found for a particle size of 10 μm, indicating that the particles of this size are most affected by the fluid drag force; this phenomenon is more clearly evident for low surface energy. Under the action of AC voltage, when the particle size changes from small to large, the amounts of contamination

for the low surface energy are 50–63%, 58–86%, 27–65% and 28–78% lower than that of the original surface energy. Therefore, reducing the surface energy of the sheds in the AC transmission line can also effectively improve the contamination of the insulator sheds area.

The ratio of DC and AC contamination accumulation of the porcelain double umbrella insulator for the two kinds of surface energy is shown in Fig. 9.

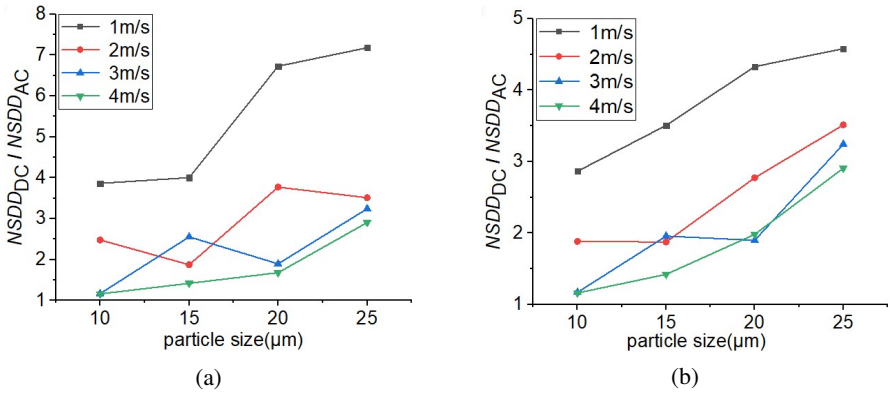

Fig. 9. The ratio of DC and AC contamination accumulation of porcelain double umbrella insulators under two kinds of surface energy: original surface energy (a); low surface energy (b)

As observed from Fig. 9, for the same wind speed, the ratio of DC and AC contamination accumulation gradually increases with the increase in particle size because with the increase in particle size, the fluid drag force, electric field force and gravity of the particles increase, and the increase in electric field force is greater. Compared with the same particle size, the ratio of DC and AC contamination accumulation decreases gradually with the increase in wind speed, and the influence of fluid drag force is greater at this case. Under the action of DC voltage, the action of the electric field force on the particles to a certain extent increases the probability of particle deposition, while for the AC voltage, the periodic variation of the field strength changes the direction of the electric field force when the particles move in space, so that the effect of the electric field force on the particles over the entire AC cycle is almost zero. A comparison of Fig. 9(a) and Fig. 9(b) shows that for: low surface energy, the adsorption effect of the shed on particles is greatly reduced. In this case, the particles are mainly affected by the fluid drag force, electric field force and gravity when the particle size changes. Therefore, the overall change trend of the curve in Fig. 9(b) is gentler than that of the curve in Fig. 9(a).

5. Conclusions

In this study, the surface energy is considered the influencing factor for the first time in the study of insulator contamination characteristics. After analyzing the effect, it is introduced into the deposition criterion formula, and the rationality of the modified model is verified by comparing the results of the wind tunnel test and numerical simulation. In addition, the similarities and

differences in natural contamination characteristics of porcelain double umbrella insulators under different surface energy are compared and analyzed. The conclusions and prospects are as follows:

1. Due to differences in settling forces of particles with different particle sizes, the amount of contamination on the insulator surface first decreases and then increases with increasing particle size under two kinds of surface energy.
2. Compared with the 10 μm particle size, the amounts of contamination for the original surface energy and the low surface energy of 15 μm particle size decreases by approximately 60–81% and 80–93%, respectively, in this case the low surface energy is relatively less attractive to the particles in the normal direction.
3. The amounts of contamination for the low surface energy are 64–75%, 60–95%, 55–91% and 54–78% lower than those for the original surface energy for particle sizes of 10, 15, 20 and 25 μm. Therefore, it is recommended to use insulators with low surface energy in areas with larger particle sizes of contamination particles, so as to effectively reduce the surface pollution of insulators and ensure the safe operation of the line.
4. For the same particle size, the ratio of DC and AC contamination accumulation decreases gradually with the increase in wind speed, and the influence of the fluid drag force is greater in this case. Through the amplitude of the two changes, the influence of the drag force or the electric field force under each work condition can be effectively analyzed.
5. In this study, the contamination characteristics of insulators with different surface energy under common work conditions are studied, but the regionality of insulator work is strong. For example, the types and properties of contamination particles are different in industrial areas, and their deposition on low surface energy insulator sheds is also particularly important. In the future, in-depth research on this aspect can be carried out to provide important reference for the safe operation of insulators in different regions.

References

[1] Boudissa R., Djafri S., Haddad A., Belaicha R., Bearsch R., *Effect of insulator shape on surface discharges and flashover under polluted conditions*, IEEE Transactions on Dielectrics and Electrical Insulation, vol. 12, no. 3, pp. 429–437 (2005), DOI: 10.1109/TDEI.2005.1453447.

[2] Lan L., Mu L., Wang Y., Yuan X.Q., Wang W., Li Z.H., *The influence of pollution accumulation on coating aging of UHV line insulators with different suspension height in coal-ash polluted area*, Archives of Electrical Engineering, vol. 69, no. 1, pp. 39–56 (2020), DOI: 10.24425/aee.2020.131757.

[3] Yang L.G., Pauli F., Zhang S.M., Hambrecht F., Hameyer K., *Influence of conductive particle contamination on the insulation system of rotating electrical machines with direct oil cooling*, Archives of Electrical Engineering, vol. 71, no. 3, p. 789–804 (2022), DOI: 10.24425/aee.2022.141685.

[4] Fan C., Zhang X.Q., Guo Y.J., Li C.M., Liu Y.J., Wu G.N., *Study on Accumulation of Contamination Particles on Surface of Insulating Materials*, High Voltage Apparatus, vol. 58, no. 11, pp. 212–220 (2022).

[5] Li J.Y., *Regulation technology of ceramic surface free energy and its easy-cleaning property*, Master's Thesis, Materials Physics and Chemistry, Hebei University of Technology, Tianjin (2007).

[6] Hu S.H., Liang J.S., Sun D.Y., Wang L.J., Wang F., *Effect of surface free energy on easy-to-clean property of ceramic glaze*, Journal of the Chinese Ceramic Society, vol. 36, no. 9, pp. 1282–1287 (2008), DOI: 10.14062/j.issn.0454-5648.2008.09.008.

[7] Wang J., Li Y., Liang X.D., Liu Y.Y., *Research of adhesion force between dust particles and insulator surface using atomic force microscope*, High Voltage Engineering, vol. 39, no. 6, pp. 1352–1359 (2013), DOI: 10.3969/j.issn.1003-6520.2013.06.010.

[8] Xu L., Ding J.N., Xu X.J., Li B.Q., Niu X.Y., *Structure and surface energy analysis of micro-arc oxidation-hydrothermal synthesis composite ceramic coating on TA2 surface*, Rare Metal Materials and Engineering, vol. 45, no. 8, pp. 2080–2085 (2016).

[9] Jiang Y.P., *Study on Dynamic Behavior Characteristics of Particle on Insulator Surface under Strong Electric Field*, Master's Thesis, Electrical Engineering, Huazhong University of Science and Technology, Wuhan (2019).

[10] Zhang X.Q., Fan C., Guo Y.J., Liu K., Liu Y.J., Wu G.N., *Microscopic Distribution of Polluted Particles on the Surface of Insulating Materials*, Power System Technology, vol. 44, no. 3, pp. 1180–1187 (2020), DOI: 10.13335/j.1000-3673.pst.2019.1589.

[11] He Z.H., Gao F., Tu Z.F., Zhang Y.C., Chen H., *Analysis of natural contamination components and sources of insulators on ±800 kV DC lines*, Electric Power Systems Research, vol. 167, pp. 192–198 (2019), DOI: 10.1016/j.epsr.2018.10.033.

[12] Gao S., Liu Y., Cao B., Chen J., Gao S.M., Wang L.M., *Research on the Cleaning Effect of Natural Rainfall on the Naturally Contaminated Insulators*, Insulators and Surge Arresters, vol. 298, no. 6, pp. 159–163 (2020).

[13] Zhang Z.J., Zhang D.D., Jiang X.L., Liu X.H., *Study on Natural Contamination Performance of Typical Types of Insulators*, IEEE Transactions on Dielectrics and Electrical Insulation, vol. 21, no. 4, pp. 1901–1909 (2014), DOI: 10.1109/TDEI.2014.004343.

[14] Tu Y.P., Sun Y.F., Peng Q.J., Wang C., Gong B., Chen X.F., *Particle size distribution characteristics of naturally polluted insulators under the fog-haze environment*, High Voltage Engineering, vol. 40, no. 11, pp. 3318–3326 (2014), DOI: 10.13336/j.1003-6520.hve.2014.11.004.

[15] Lv Y.K., Chen Z.Z., Ge Q.Z., Wang Q., Zhang Y.Z., *Numerical Simulation of Contamination Accumulation Characteristics of Composite Insulators in Salt Fog Environment*, Energy Engineering: Journal of the Association of Energy Engineering, vol. 120, no. 2, pp. 483–499 (2023), DOI: 10.32604/ee.2023.023649.

[16] Elimelech M., Gregory J., Jia X., *Particle deposition and aggregation: measurement, modelling and simulation*, Butterworth-Heinemann (1995).

[17] Lv Y.K., Li J.G., Zhang X.M., Pang G.L., Liu Q., *Simulation study on contamination accumulation characteristics of XP13-160 porcelain suspension disc insulators*, IEEE Transactions on Dielectrics and Electrical Insulation, vol. 23, no. 4, pp. 2196–2206 (2016), DOI: 10.1109/TDEI.2016.7556495.

[18] Lv F.C., Huang H., Liu Y.P., Qin C.X., Liu Q., Xu T., *Contamination depositing characteristics of insulators under natural crosswind conditions with wind tunnel simulation*, High Voltage Engineering, vol. 40, no. 5, pp. 1281–1289 (2014), DOI: 10.13336/j.1003-6520.hve.2014.05.001.

[19] He B., Jin H.Y., Gao N.K., Gao N.K., Chen B.F., Peng Z.R., *Characteristics of dust deposition on suspended insulators during simulated sandstorm*, IEEE Transactions on Dielectrics and Electrical Insulation, vol. 17, no. 1, pp. 100–105 (2010), DOI: 10.1109/TDEI.2010.5412007.

[20] Li J.G., *Simulation Study on Contamination Accumulation Characteristics of Porcelain Insulators in Strong Wind*, Master's Thesis, Energy Power and Engineering, North China Electric Power University, Baoding (2017).

[21] Liu Y.M., Shi J.Y., Lu Q.Q., Guo Y.Z., Chen R.Q., Yin D.C., *Research Progress on Calculation of Solid Surface Tension Based on Young's Equation*, Materials Reports, vol. 27, no. 11, pp. 123–129 (2013).

[22] Xu A.M., Zeng L.K., *Development of hydrophobic ceramic surface*, Journal of Synthetic Crystals, vol. 36, no. 2, pp. 405–409 (2007), DOI: 10.16553/j.cnki.issn1000-985x.2007.02.036.

[23] Li L.H., Zheng C., *Progress in Antifouling Self-Cleaning Coatings in China*, Coating and Protection, vol. 35, no. 7, pp. 23–28 (2014).

[24] White H.J., *Industrial electrostatic precipitator*, Reading UK: Addison-Wesley (1963).

[25] Packham D.E., *Surface energy, surface topography and adhesion*, International Journal of Adhesion and Adhesives, vol. 23, no. 6, pp. 437–448 (2003), DOI: 10.1016/S0143-7496(03)00068-X.